IEEE Access
Multidisciplinary | Rapid Review | Open Access Journal

Received 22 January 2026, accepted 8 February 2026, date of publication 23 February 2026, date of current version 2 March 2026.

Digital Object Identifier 10.1109/ACCESS.2026.3666451

APPLIED RESEARCH

Dynamic State-of-Charge Modeling in Battery Energy Storage Systems With Power Ramp-Rate Control

ANDRÉ FERNANDO SCHIOCHET[1,2], GUSTAVO JACQUES FRIEDRICH[2,3], JOÃO ALBERTO PASSOS FILHO[1], AND JANAíNA GONÇALVES DE OLIVEIRA[1,4]

[1]Department of Electrical Energy, Federal University of Juiz de Fora, Juiz de Fora, Minas Gerais 36036-900, Brazil
[2]Petróleo Brasileiro S.A., Rio de Janeiro, Rio de Janeiro 20231-030, Brazil
[3]Electrical Engineering Department, Federal University Fluminense, Niterói, Rio de Janeiro 24210-240, Brazil
[4]Department of Electrical Engineering, Division for Electricity, Uppsala University, 752 37 Uppsala, Sweden

Corresponding author: André Fernando Schiochet (andre.schiochet@estudante.ufjf.br)

This work was supported in part by the National Research Council (CNPq), in part by Brazilian Federal Agency for Support and Evaluation of Graduate Education (CAPES)—Finance Code 001, in part by the State of Minas Gerais Research Foundation (FAPEMIG), in part by the Federal University of Juiz de Fora (UFJF), in part by the National Institute of Science and Technology in Electric Energy (INERGE), and in part by PETROBRAS.

ABSTRACT This paper presents a vectorized approach for modeling and tuning the state-of-charge (SOC) dynamics in Battery Energy Storage Systems (BESS) equipped with power ramp-rate control (PRRC). The SOC evolution is formulated in discrete time, and parameter estimation is performed using Differential Evolution (DE) integrated with Anatem, a dynamic simulation tool used for electromechanical transient studies. This study compares the traditional generic (WECC-based) SOC model, which employs a fixed-gain integrator, with a proposed variable-gain integrator that adapts to BESS active power through a piecewise-linear function. The methodology is validated using real SCADA data from a 1.1-MW photovoltaic plant coupled with a 0.95-MW/0.49-MWh BESS in Brazil. Measurements were sampled at 1-second intervals, while Anatem simulations employed a 50-ms integration step to ensure numerical accuracy and appropriate representation of converter-level dynamics. A reference day and multiple operational scenarios were used for calibration and cross-validation. Results show that the variable-gain formulation reduces the Root Mean Square Error (RMSE) by 57–91% compared with the standard generic model, providing an improved fidelity during rapid charge and discharge transitions. The method also enhances the alignment between simulated and measured active-power behavior, supporting robust ramp-rate compliance and improved representation of BESS operational limits. The proposed framework is suitable for both short-term dynamic simulations and long-term operational analyses and can be extended to hybrid configurations and other control functions that require parameter tuning from real operational data. The findings highlight the importance of dynamic gain adaptation for accurate SOC modeling in hybrid PV–BESS systems and support the applicability of this method in stability studies, operational planning, and hybrid system design.

INDEX TERMS Battery energy storage systems, differential evolution, energy management, optimization, parameter estimation, power system modeling, ramp-rate control, state of charge, time-series analysis, vector optimization.

ACRONYMS

BESS	Battery Energy Storage System.
ONS	Brazilian Grid Operator.
DER	Distributed Energy Resources.

The associate editor coordinating the review of this manuscript and approving it for publication was Nagesh Prabhu.

© 2026 The Authors. This work is licensed under a Creative Commons Attribution 4.0 License.
For more information, see https://creativecommons.org/licenses/by/4.0/

WECC	Western Electricity Coordinating Council.
SOC	State of Charge.
PRRC	Power Ramp Rate Control.
RMSE	Root Mean Square Error.
DE	Differential Evolution.
PPC	Plant Power Controller.
POI	Point of Interconnection.
REPC	Renewable Energy Plant Controller.
REEC	Renewable Energy Electrical Control.
REGC	Renewable Energy Generator Control.
SOH	State of Health.
RR_control	Ramp-rate Control Module.
SOH	State of health of the battery (pu).

SYMBOLS AND VARIABLES

P_{POI}	Active power at the Point of Interconnection (MW or pu).
P_{PV}	PV active power (MW or pu).
P_{PV}^{meas}, P_{PV}^{calc}	Measured and calculated PV active power.
P_{Bess}	BESS active power (MW or pu).
$P_{Bess,i}$	BESS active power at time index i.
E_{rated}	Nominal energy capacity of the battery (MWh).
η_{PCS}	Power converter efficiency (pu).
η_{bat}	Battery efficiency (pu).
Δt	Simulation sampling interval (s).
$s\,[i]\,or SOC_i$	State of charge at time index i (pu).
SOC_{ini}	Initial state of charge (pu).
SOC_{min}, SOC_{max}	Minimum and maximum allowable SOC (pu).
$t = [t_1, t_2, \ldots, t_N]^T$	Discrete simulation time grid (s).
N	Number of time steps.
θ	Vector of model parameters.
s_{meas}	Vector of measured SOC values (pu).
$s_{calc}\,(\theta)$	Vector of simulated SOC values (pu).
$e\,(t, \theta)$	SOC residual vector: measured minus simulated (pu).
$F_{obj}\,(\theta)$	Objective function: RMSE of SOC tracking (pu).
$RMSE_{SOC}$	SOC tracking RMSE (pu).
T	SOC time constant (s).
T_{min}, T_{max}	Lower and upper bounds for T (s).
$T_{initial}$	Initial time constant estimated from Eq. (3) (s).
P_1, P_2, P_3, P_4	Parameters of the variable gain ramp function.
k_{pvar}	Variable gain applied to the SOC integrator.
$RR_{\max}$, $RR_{\min}$	Ramp rate limits at the POI (pu/s).
K_{p_g}, K_{i_g}	PRRC proportional and integral gains.
T_{lag}, T_p, T_{pK}	Time constants used in PRRC and freeze logic (s).

I. INTRODUCTION

Battery energy storage systems (BESS) play a crucial role in stabilizing power systems that incorporate high levels of variable renewable energy sources. BESS offers fast response, flexibility, predictability, and multiple services such as ramp-rate control, frequency regulation, voltage control, energy arbitrage, and curtailment avoidance in hybrid plants [1], [2], [3].

According to the Brazilian grid operator (ONS), cascading disconnections occurred in distributed energy resources (DER) from 2021 to 2024 [4], partly due to an inadequate model response. This highlights the challenge of developing robust control mechanisms for renewable intermittency in photovoltaic (PV) systems. Accurate multi-scale modeling, from seconds to years, is essential for effective planning [5].

Western Electricity Coordinating Council (WECC) second-generation generic models are common in phasor-domain stability simulations [6], [7], [8], [9], [10], but they have limitations. They only cover 0.1–10 Hz, have reduced accuracy in weak grids (short-circuit ratio below 2–3), and use a simplified state of charge (SOC) representation for long simulations [11], [12]. SOC indicates the battery energy as a percentage of the total capacity.

Although it is assumed that the SOC variation is negligible in transient stability [13], explicit SOC modeling is important for operational flexibility and for linking short to long-term analyses. Few studies have assessed the accuracy of generic SOC models using long-term simulations. Sensitivity to input resolution (granularity) has rarely been examined. As noted in [5], 81% of sizing studies use hourly data; few use minute- or second-level resolution, which limits the precision of the dynamic simulation.

Recent advances in energy storage system optimization and control have addressed key challenges in sizing, operation, and dynamic management. Shi et al. [14] proposed a modified biogeography-based optimization strategy for optimal sizing and performance of battery energy storage systems in microgrids with wind energy penetration, demonstrating that adaptive algorithms and consideration of battery depth of discharge and lifespan are crucial for economic and reliable operation. While their approach is effective for planning and resource allocation, it relies on simulated scenarios and does not address dynamic modeling of state of charge (SOC) or real-time control using operational data. Maroufi et al. [15] introduced a moving average and fuzzy logic-based power management strategy for hybrid flywheel-battery energy storage systems, emphasizing real-time SOC and ramp-rate management with experimental validation. However, their work is centered on hybrid topologies and adaptive power sharing, without exploring detailed SOC modeling or automated parameter tuning in PV–BESS plants. Li and Ghiasi [16] presented a mathematical strategy for economic virtual power plant (VPP) utilization in electricity markets, considering the effects of energy storage and ancillary services. Their model optimizes trading and resource dispatch in VPPs, highlighting the economic benefits of integrating

energy storage, but focuses primarily on market participation and does not investigate high-resolution SOC modeling or dynamic calibration with real operational data.

In contrast, the present work critically evaluates the accuracy of generic SOC models in long-term dynamic simulations using real SCADA data from a hybrid PV–BESS plant, and proposes an automated parameter tuning framework capable of adapting to diverse operational scenarios and time resolutions. By bridging the gap between economic planning, experimental validation, and dynamic modeling, this approach advances the state of the art for hybrid energy storage systems in real-world applications, with particular emphasis on robust SOC tracking and ramp-rate control for stability studies during contingencies.

Beyond PV–BESS plants, the proposed SOC modeling and optimization framework is compatible with hybrid AC/DC microgrids featuring bidirectional power transfer and electric-vehicle (EV) participation. In such settings, SOC-aware storage management can complement hierarchical converter control and reactive-power coordination, as discussed in recent work on hybrid AC/DC architectures [17].

A. MOTIVATION AND CONTRIBUTION OF THIS WORK

In this context, the main contributions are: (i) a critical evaluation of generic SOC model accuracy in long simulations, (ii) an automated tuning framework for diverse scenarios, (iii) SOC analysis at 1-second time steps, and (iv) insights for stability studies during contingencies when stored energy aids recovery.

This study applies power ramp rate control (PRRC) in a hybrid PV–BESS plant and compares the standard and variable-gain SOC models. The models were implemented in Anarede v12.0.1 and Anatem v12.7.0 [18]. Both programs are product-grade software developed by Brazilian Electric Energy Research Center (CEPEL).

Anarede is a computational tool for steady-state power flow and short-circuit analysis, and is widely used for planning and operation studies in Brazilian power systems. Anatem (Electromechanical Transient Analysis – in Portuguese: Análise de Transitórios Eletromecânicos) is a dynamic simulation application designed for fundamental frequency stability studies, enabling time-domain analysis of electromechanical transients in power system operation and planning.

The generic WECC model was selected as the baseline due to its broad international acceptance and, most importantly, its compatibility with the technical requirements recently published by the ONS (NT-ONS DPL 0111/2025) [19]. This document requires that mathematical models for battery energy storage systems be open, parameterizable, and compatible with the main simulation tools used in Brazil, such as Anatem and PSCAD® [20].

The main methodological innovation of this work lies in the adaptation and extension of the WECC model for long-term analyses and industrial scenarios. By adjusting the SOC parameters and control logic, the model's application is expanded beyond grid integration to include operational planning and performance evaluation in diverse contexts.

The proposed methodology integrates Python-based optimization with Anarede and Anatem simulations, using the SciPy Differential Evolution (DE) algorithm v1.16.2 [21]. The DE algorithm was employed to minimize an objective function defined as the Root Mean Square Error (RMSE) between the measured and simulated state of charge profiles. Vectorized population generation supports parallel simulations for greater efficiency. The model parameters were tuned to minimize the RMSE between the measured and simulated SOC with high-resolution SCADA data.

The remainder of this paper is organized as follows. Section I presents the introduction, including the motivation and main contributions of this study. Section II describes the proposed methodology, detailing the modeling approach, parameter tuning, and integration of Python-based optimization with Anarede and Anatem simulations. Section III discusses the test system and data used for model calibration and validation. Section IV presents and analyzes the results obtained from the optimization and simulation studies. Finally, Section V provides the main conclusions and outlines directions for future research.

II. PROPOSED METHODOLOGY

This section outlines the methodology for the modeling and parameter tuning of the generic models used for the hybrid PV–BESS plant. Specifically, it covers the PRRC implemented in the plant power controller (PPC) and the SOC model, including both generic and proposed versions.

A. HYBRID PLANT MODEL

The test system configuration followed [7] and the UFV-AR hybrid plant from northeastern Brazil. The hybrid system consisted of a 1.1 MW photovoltaic (PV) array matched with a 0.95 MW/0.49 MWh lithium-ion BESS at a C-rate of 2. The simplified single-line diagram (Fig. 1) shows five buses, transformers, and equivalent lines. Buses 1 and 11 operate at 0.6 kV; buses 2 and 3 at 13.8 kV; and bus 4 at 230 kV. Transformers (1–2), (11–2), (3–4), and line 2–3 have reactances of X = 0.0001 pu (100 MVA base). The point of interconnection (POI) is bus 2, where the measurements and control actions are performed. Using (1), we calculate the active power balance as follows:

$$P_{POI} = P_{PV} + P_{Bess} \tag{1}$$

P_{POI} represents the active power measured at the point of interconnection, P_{PV} denotes the active power generated by the photovoltaic system, and P_{Bess} denotes the active power supplied by the BESS.

The dynamic behavior of a hybrid plant is captured using second-generation generic models for Renewable Energy Systems (RES). These models are structured into three main functional blocks [6], [9], [13], [22]:

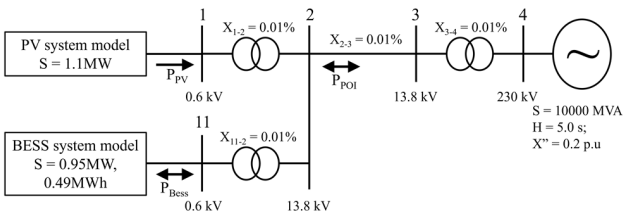

FIGURE 1. 5-bus test system.

- REPC Module (Renewable Energy Plant Controller): Implements plant-level control functions, acting as a PPC to coordinate multiple renewable sources. The REPC module generates active and reactive power references (target values for the amount of real and reactive electrical power to be produced), regulates the voltage at the POI, and provides frequency control through active power adjustments. In this study, the PRRC module, as presented in [23], is adopted to enable advanced functionalities such as ramp rate control (PRRC, a method that limits how quickly the power output can change), allowing the BESS to smooth generation ramps and mitigate fluctuations in PV output on the grid.
- REEC Module (Renewable Energy Electrical Control): Implements internal electrical control for the power converter. The power converter manages the conversion between electrical power forms (e.g., AC and DC). The REEC translates active and reactive power references, usually from the plant controller (REPC), into inverter current commands. It operates in a closed loop with the REGC module, overseeing the current injection based on the voltage and power inputs. The REEC maintains converter current limits and priority logic to decide which power (active or reactive) is prioritized. REEC_B was applied to the PV systems. REEC_C is tailored for BESS and includes battery charge/discharge management and SOC modeling, which were evaluated in this study.
- REGC Module (Renewable Energy Generator Control): Models the interface between the renewable generator and grid. It represents the current injection behavior of inverter-based resources, such as PV, BESS, and wind. The module emulates fast-acting current control of the converter by rapidly regulating the current output. It responds to voltage and frequency changes, ensuring compliance with the grid requirements for fault ride-through and dynamic performance. It operates in a closed loop with the REEC module, converting the current commands into grid injections.

Generation controllers (REGC_A), electrical converters (REEC_B and REEC_C), and plant controller (REPC_A) were used to represent the PV and BESS models in the hybrid plant simulations, as shown in Fig. 2.

While SCADA measurements of PV active power (P_{PV}^{meas}) were available, the BESS model uses the internally calculated PV power (P_{PV}^{calc}) as the reference for the PRRC ($RR_{control}$). This choice ensures full consistency among all dynamic blocks of the simulation, since the PV, PRRC, and BESS models operate under the same assumptions, sampling structure, and internal delays. When the measured signal is used directly, small timing differences inherent to SCADA acquisition and controller execution may reduce the correlation between measured PV power and simulated BESS response. Using the internally computed PV power avoids such timing mismatch and preserves the internal coherence of the simulation framework.

The outputs of the BESS model are as follows: (*i*) the calculated BESS active power (P_{Bess}^{calc}), which ensures ramp-rate compliance (MW/min) at the POI within the specified limit; (*ii*) the calculated BESS SOC (SOC_{Bess}^{calc}), maintained within the minimum and maximum bounds; and (*iii*) the calculated POI active power (P_{POI}^{calc}), which is represented by the sum of the PV and BESS active powers.

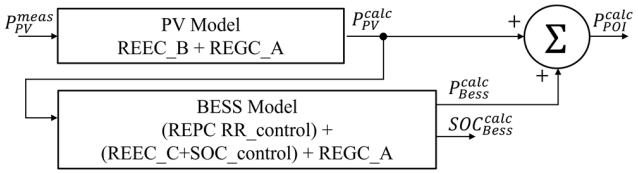

FIGURE 2. Represents a PV plant associated with BESS for ramp-rate control.

Block diagrams of the PV and BESS models, along with their network connections, are shown in Figs. 3 and 4, which represents the hybrid PV–BESS plant. Fig. 3 illustrates the connection between the REEC_B and REGC_A modules in the PV generic model. Fig. 4 shows the modules representing the BESS based on generic models and additional components. The highlighted blocks correspond to the PRRC block embedded in the REPC_A module and SOC model evaluated in this study.

It is important to point out that although the block diagrams include reactive power control modules, the focus of the model and this study was on the active power ramp rate control. The reactive power was not actively controlled and was assumed constant throughout the simulations. Therefore, no impact on the reactive power was observed.

Although the WECC generic model was originally developed for short-term dynamic studies, in this work we adapt and calibrate its parameters, especially SOC and ramp rate control logic, to enable long-term operational analyses and behind-the-meter scenarios, in compliance with the latest ONS technical requirements (NT-ONS DPL 0111/2025) [19]. This methodological innovation allows the same model, already validated and accepted by ONS, to be used for extended simulations and decentralized applications.

B. SOC MODELS

1) GENERIC SOC MODEL

The generic SOC model (Fig. 5) employs a fixed-gain integrator defined by a time constant T, which governs the

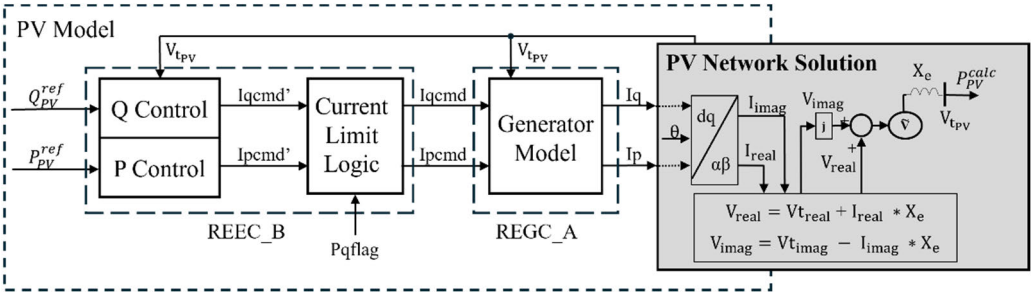

FIGURE 3. PV model considering the generic blocks (REEC_B +REGC_A). Source: Author, adapted from [12].

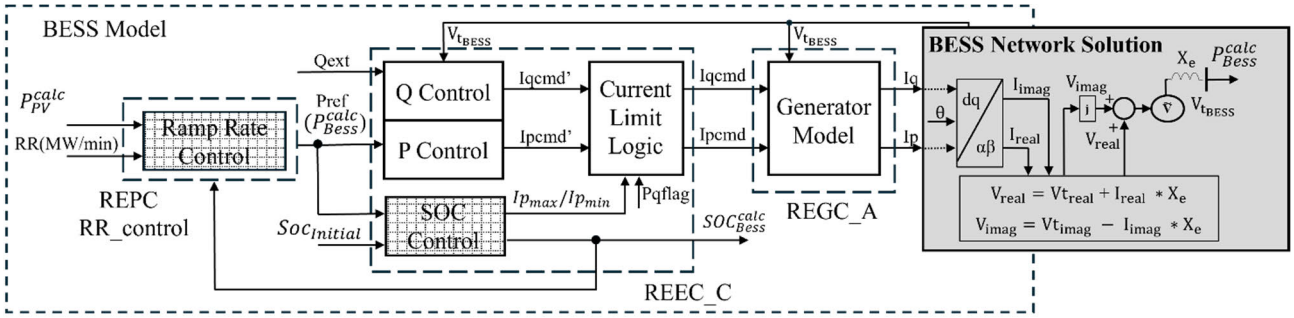

FIGURE 4. BESS model with PRRC in REPC_A and SOC control in REEC_C.

charge and discharge dynamics. The model receives the initial SOC (SOC_ini) as input and the calculated BESS active power (P^{calc}_{Bess}). Operational boundaries were enforced through the minimum and maximum SOC limits (SOC_{min}, SOC_{max}). When $SOC \rightarrow SOC_{min}$, the maximum current $I_{p,max}$ is set to zero, preventing further discharge ($P_{Bess} > 0$). Conversely, when $SOC \rightarrow SOC_{max}$, the minimum current $I_{p,min}$ is set to zero, preventing further charge ($P_{Bess} < 0$).

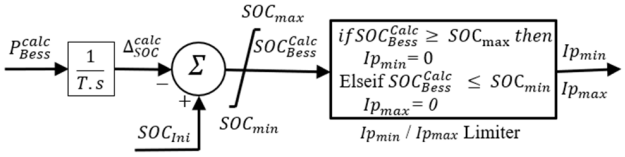

FIGURE 5. Generic SOC model block diagram. Source: Author, adapted from [12].

The internal battery and converter dynamics, such as the detailed switching behavior, control loops, and transient responses, were not explicitly modeled within the SOC controller block. Instead, the SOC model operates as an equivalent system in which the converter and battery are represented in a simplified manner.

The fast current control and grid interface dynamics of the converter are managed by the REGC module, which emulates the current-injection behavior of inverter-based resources and responds to voltage and frequency events. Thus, the SOC model focuses solely on the energy balance and operational limits, while the REEC and REGC blocks manage the dynamic response of the converter.

The SOC energy balance was computed using (2), and the theoretical time constant T was derived from (3).

$$SOC_{i+1} = SOC_i + \frac{P_{Bess,i} * \Delta t}{T} \tag{2}$$

$$T = \frac{E_{Bess,rated} * SOH * \eta_{PCS} * \eta_{bat} * 3600}{C - rate * P_{PCS,rated}} \tag{3}$$

where:

- SOC_i: State of charge at time step i(pu, per unit)
- $P_{Bess,i}$: BESS active power at time step i (pu)
- $\Delta t = t_{i+1} - t$: Sampling interval (s)
- T: Charge and discharge time constant (s)
- $E_{Bess,rated}$: Nominal battery capacity (MWh)
- SOH: State of health of the battery (pu)
- η_{PCS}: Power converter efficiency (charge and discharge) (pu)
- η_{bat}: Battery efficiency (charge and discharge) (pu)
- $C - rate$: A dimensionless parameter that quantifies the rate at which a battery is charged or discharged relative to its maximum capacity. A C-rate of 2 (2C) indicates that the battery would be fully charged or discharged in half an hour.
- $P_{PCS,rated}$: Nominal active power of the equivalent power converter (MW)

In this work, both battery and converter efficiencies are represented by a single, constant value embedded within the time constant T of the generic SOC model. This approach

does not explicitly differentiate between charging and discharging efficiencies, nor does it account for temperature or SOH dependence, which are typically neglected in aggregated system-level models for computational efficiency and long-term analysis.

Although adjusting T based on (3) improves the accuracy for specific days, the model lacks generalization in long-term simulations. This limitation is attributed to the absence of nonlinear battery and converter phenomena, such as the modified Peukert effect, nonlinear Joule heating, concentration polarization, and voltage-SOC hysteresis, all of which are not captured by the linear integrator approach [24], [25], [26].

2) PROPOSED SOC MODEL WITH VARIABLE GAIN

The proposed SOC model introduces a variable gain block (k_p^{var}) preceding the integrator (Fig. 6), which is dynamically adjusted using a ramp function based on the magnitude of the BESS active power (P_{Bess}). This mechanism effectively modulated the integration time constant and enhanced the responsiveness of the model to power fluctuations.

The ramp function parameters (P_1, P_2, P_3, P_4) expressed in (4), were tuned to reflect the physical relationship between power demand and SOC variation. Specifically, the function is piecewise-linear, implemented through two consecutive ramp segments that define three operating regions:

- Region 1: For $P_{Bess} \leq P_1$, the gain remains constant at P_2.
- Region 2: For $P_1 < P_{Bess} < P_3$, the gain varies linearly between P_2 and P_4.
- Region 3: For $P_{Bess} \geq P_3$, the gain remains constant at P_4.

This approach introduces only four parameters compared to the single constant gain of the traditional WECC integrator, ensuring minimal complexity while improving dynamic accuracy. The chosen breakpoints (P_1, P_3) and gain levels (P_2, P_4) were calibrated to represent the nonlinear SOC consumption behavior under varying power conditions. The time constant T was adjusted according to (3).

$$k_p^{var} = \begin{cases} P_2 & if\ P_{Bess} \leq P_1 \\ P_2 + \dfrac{P_4 - P_2}{P_3 - P_1} * (P_{Bess} - P_1) & if\ P_1 < P_{Bess} < P_3 \\ P_4 & if\ P_{Bess} \geq P_3 \end{cases} \tag{4}$$

This dynamic adjustment improves the tracking accuracy during charge/discharge cycles, particularly under variable operating conditions, while maintaining compatibility with WECC guidelines and practical implementation in Anatem through the ramp block.

C. OPTIMAL PARAMETER ADJUSTMENT

To ensure that the proposed models accurately represent the real BESS operation data, an optimization routine was

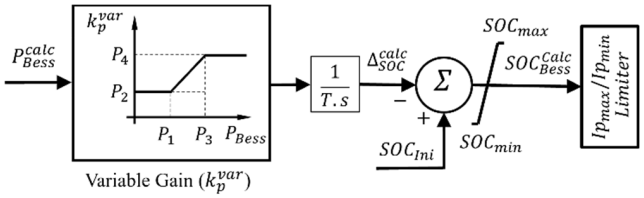

FIGURE 6. Proposed SOC model (REEC_C) with variable gain.

implemented using the DE method. The DE algorithm was employed to minimize an objective function defined as the RMSE between the measured and simulated SOC profiles. The configuration uses a vectorized activated option, enabling parallel evaluation of candidate solutions and significantly reducing the computational time. This approach is efficient when integrated with the Anatem program because it allows for the simultaneous assessment of multiple scenarios.

Let the discrete time vector be:

$$\boldsymbol{t} = [\boldsymbol{t_1}, \boldsymbol{t_2}, \ldots, \boldsymbol{t_N}]^{\boldsymbol{T}}\ (\boldsymbol{seconds})$$

Denote the measured and simulated SOC vectors as:

$$\boldsymbol{s^{meas}}(\boldsymbol{t}), \boldsymbol{s^{calc}}\left(\boldsymbol{P_{Bess}^{calc}}(\boldsymbol{t}), \boldsymbol{\theta}\right) \in \mathbb{R}^n$$

where θ represents the set of model parameters to be optimized (e.g., T for the generic model, or P_1, P_2, P_3, P_4 for the variable gain model).

The calculated BESS active power $\boldsymbol{P_{Bess}^{calc}}(\mathbf{t})$ is also a time-dependent quantity and results from the PRRC model (Fig. 4). Accordingly, the simulated SOC $\boldsymbol{s^{calc}}(\boldsymbol{t})$ at each time step depends on the entire sequence of BESS active power values over time as well as on the parameter set θ.

The error vector is defined in (5) as a function of time and parameters.

$$\boldsymbol{e}(\boldsymbol{t}, \boldsymbol{\theta}) = \boldsymbol{s^{meas}}(\boldsymbol{t}) - \boldsymbol{s^{calc}}\left(\boldsymbol{P_{Bess}^{calc}}(\boldsymbol{t}), \boldsymbol{\theta}\right) \tag{5}$$

where $\boldsymbol{e}(\boldsymbol{t}, \boldsymbol{\theta}) \in \mathbb{R}^n$ and each element $e_i(\theta)$ corresponds to the error at the time t_i.

The objective function is the RMSE between the measured SOC ($\boldsymbol{SOC_{Bess}^{meas}}$) and calculated ($\boldsymbol{SOC_{Bess}^{calc}}$) vectors, as defined in (6):

$$F_{obj}(\theta) = RMSE_{SOC}(\theta) = \sqrt{\frac{1}{N}\sum_{i=0}^{N}\left(SOC_{Bess,i}^{meas} - SOC_{Bess,i}^{calc}(\theta)\right)^2} \tag{6}$$

where N is the number of time steps in the discrete grid $\boldsymbol{t}$, and all symbols are defined by acronyms.

Operational constraints, such as ramp-rate limits and SOC bounds, were enforced as parameter bounds and simulation conditions, but were not included as penalty terms in the objective function.

1) GENERIC MODEL OPTIMIZATION

For the generic SOC model, the parameter set is reduced to a single scalar T, and the optimization problem is shown in (7).

$$\begin{aligned} &min\ F_{obj}(T) \\ &subject\ to:\ T_{min} \leq T \leq T_{max} \end{aligned} \tag{7}$$

where T_{min} and T_{max} are the bounds derived from the theoretical value of T (see (3)).

2) VARIABLE GAIN MODEL OPTIMIZATION

For the variable gain SOC model, the optimization expands to include ramp function parameters, as shown in (8). Operational constraints were implemented with a small positive tolerance (ε), to avoid strict equality and ensure numerical robustness. These constraints ensure physical plausibility and numerical stability of the ramp function used to modulate the SOC integration gain.

$$\begin{aligned} &min\ F_{obj}(P_1, P_2, P_3, P_4) \\ &subject\ to:\ P_1 \geq P_{1,min} + \varepsilon \\ &\qquad P_2 \geq \varepsilon \\ &\qquad P_3 \geq P_{3,min} + \varepsilon \\ &\qquad P_4 \geq P_{4,min} \\ &\qquad P_1 < P_3 < P_{3,max} \\ &\qquad P_2 < P_4 < P_{4.max} \\ &\qquad P_1 - P_3 \leq -\varepsilon \\ &\qquad P_2 - P_4 \leq -\varepsilon \end{aligned} \tag{8}$$

- ε is a small positive tolerance (e.g., 10^{-3}), which is used to avoid strict equality constraints and ensure numerical feasibility.
- $P_{3,max}$ and $P_{4,max}$ are the upper bounds for P_3 and P_4.
- $P_{3,min}$ and $P_{4,min}$ is the lower bound for P_3 and P_4.

D. PROPOSED METHODOLOGY DESCRIPTION

The proposed methodology for optimal SOC model parameter adjustment consists of three main steps:

Step 1: Preprocessing and Base Day Selection

- Input: Measured active power from PV, BESS, and SOC.
- Filtering: Periods with solar generation below 50 kW (≈4.5% of the PV capacity), as well as intervals exhibiting low correlation between P_{Bess} and the observed SOC evolution, were removed to ensure that only consistent operating conditions were used in the calibration stage.
- Adjustment Day: A representative day was selected, characterized by significant SOC variation, to serve as the basis for model calibration.
- Power Ramp-Rate: The ramp rate is provided as an input parameter; however, it must be validated against the measured values at the POI to ensure its adequacy and consistency with actual system behavior.

SCADA measurements were acquired at 1-second intervals, and no additional interpolation was performed by the authors. The dataset was downloaded in CSV format already interpolated by the SCADA system. Prior to model calibration, the data underwent preprocessing steps including offset removal, validation of the plant controller's calculation method, and assessment to ensure that no auxiliary controls were triggered, such as SOC charging at the end of the day. These procedures guaranteed the integrity and consistency of the operational data used for parameter estimation and model validation. The reference cases selected for model calibration and validation exhibited compliance above 99.9% with the specified ramp-rate limits, meaning that the active power delivered at the POI adhered to the ramp-rate constraint for more than 99.9% of the time during each measurement day.

The difference between the SCADA sampling interval (1 second) and the simulation integration step (50 ms) reflects the distinct requirements of steady-state data analysis and dynamic system modeling. While ramp-rate constraints themselves can be represented with coarser time steps, the 50 ms integration step is essential to accurately capture the fast response of internal control blocks, such as converter control loops and dynamic system actions. This finer resolution ensures the fidelity of transient events and control responses, enabling the model to be effectively applied to both short-term dynamic studies and long-term operational scenarios.

One notable challenge was the occasional observation of battery power variations without corresponding changes in the measured SOC. Further inspection showed that these discrepancies were not caused by sensor noise or timestamp uncertainty, but rather by operational interventions and protection actions of the BESS, such as scheduled charge/discharge routines, plant shutdown sequences, or temporary limits triggered by thermal conditions. Because these events do not represent the intrinsic SOC dynamics of the battery system, the affected intervals were removed from the dataset to ensure that only consistent operating periods were used for calibration and validation.

Step 2: Differential Evolution Configuration

The SOC model parameters were optimized using the Differential Evolution algorithm from SciPy v1.16.2. The DE configuration was selected based on empirical tests and methodological requirements to ensure robust convergence and computational efficiency. Table 1 summarizes the adopted configuration, the role of each parameter, and the rationale for its selection. A short sensitivity assessment of the DE parameters confirmed that alternative configurations produced similar RMSE values and preserved the performance advantage of the variable-gain model, indicating that the tuning is not dependent on any specific DE setup.

Parameter bounds were enforced via the SciPy bounds argument, and strict inequalities ($P_1 < P_3$, $P_2 < P_4$) were implemented as linear constraints with a small tolerance ($\epsilon = 10^{-3}$), using LinearConstraint, i.e., $P_1 - P_3 \leq -\varepsilon$ and $P_2 - P_4 \leq -\varepsilon$. Reflective mutation was not used; candidates were generated within bounds using SciPy's internal parameterization.

TABLE 1. Table summarizing DE configuration.

Parameter	VALUE	Meaning / Role in DE Algorithm	Justification /Notes
strategy	best2bin	DE mutation strategy: perturbs best solution with two difference vectors	Balances exploration and exploitation; robust for constrained search spaces.
mutation	(0.5, 1)	Range for scaling mutation factor: controls diversity in population	Randomized scaling increases diversity, reduces premature convergence.
recombination	0.7	Crossover rate: probability of mixing candidate solutions	Conventional rate; avoids instability without sacrificing RMSE.
updating	deferred	Population update method: updates after evaluating all candidates	Avoids per-trial bias; recommended for vectorized simulations.
vectorized	True	Enables parallel evaluation of candidate solutions	Reduces computational overhead, matches simulation pipeline.
polish	False	Local search refinement after DE	No significant RMSE change; maintains global optimization result and improves speed.
popsize	20	Number of candidate solutions in each generation	Balances diversity and runtime; empirically chosen.
maxiter	50	Maximum number of generations (iterations)	Ensures convergence within acceptable computational time.
tol	1e-5	Convergence tolerance: minimum change in objective function to stop	Empirically validated; ensures solution stability.
independent runs	20	Number of independent optimization runs (different seeds)	Ensures robustness and statistical reliability.
seed (per run)	seed = round_number (1…20)	Fixed random seed per independent run to guarantee reproducibility	Replaces seed=None; avoids system-entropy initialization and enables exact replication.
Generic model bounds	T_{min}=800, T_{max}=2500	Lower and upper bounds for time constant T	Ensures physical plausibility and numerical stability.
Variable gain model bounds	$[P_1, P_2, P_3, P_4]$: min=$[-1.2+\varepsilon, \varepsilon, -0.5+\varepsilon, 0.5]$, max=[0.9,10,1,1.5]	Lower and upper bounds for ramp function parameters	Ensures feasible and robust parameter search.

Step 3: Cross-Validation of Model on Multiple Days

- Generalization: The selected model and optimal parameters were applied to different days to test robustness.
- Evaluation: The SOC profiles were compared for various days under ramp rates of 5%, 10%, and 11%/min.
- Selection: The parameter set yielding the lowest total RMSE across all days was chosen to ensure the model's generalization capability.

This methodology ensures that the SOC model parameters are optimally adjusted to represent real BESS operation data, with robust validation across multiple scenarios and computational efficiency through parallelized optimization.

E. TEST SYSTEM

The data used in this study were obtained from the SCADA system of the UFV-AR hybrid PV-BESS plant following the configuration described in Section II-A and illustrated in Fig. 1.

The electrical system comprises five buses with distinct voltage levels: buses 1 and 11 operate at 0.6 kV, buses 2 and 3 at 13.8 kV, and bus 4 at 230 kV. Buses 1 and 11 were modeled as generation buses (P–V), bus 4 as a reference bus (V–θ) with a generator of significantly higher capacity than the hybrid plant, and buses 2 and 3 as load buses (P–Q). The PV array and BESS were connected to buses 1 and 11, respectively. The POI is located on bus 2, where system measurements and control actions are performed. The initial voltage and frequency at bus 4 are $V = 1.0\,pu$ and $f = 1.0\,pu$. A simulation time step of 50 ms was used.

Both the PV and BESS were represented by controlled voltage sources incorporating the control structures described in Sections II-A, II-B, and II-C. The modeling approach enables dynamic simulation of the hybrid system, including the PRRC and SOC behavior under realistic operating conditions.

The model parameters were obtained from [7], [12], [15], [16], and are detailed in Tables 2 and 3 of Appendix A – Ramp rate and WECC model parameters. These parameters include the ramp rate limits, SOC bounds, time constants, gain coefficients, and control flags used in the PRRC and SOC control blocks. Although the models did not represent the performance of a specific inverter, the parameters were tuned to replicate the measured power response of the actual UFV-AR hybrid PV–BESS system.

The optimization parameter bounds were established according to the operational constraints of the system, thereby ensuring physical plausibility and numerical stability throughout the model adjustment process.

The initial conditions and key parameters in the simulations are summarized below.

BESS Parameters:

- Rated energy: $E_{rated} = 0.49$ MWh
- State of health: SOH $= 0.93$
- Power conversion system efficiency: $\eta_{PCS} = 0.986$
- Battery efficiency: $\eta_{bat} = 0.925$
- T (time constant): $T_{initial} = 1496.2$ s (based on (3))
- Ramp-rate limit: 100 kW/min
- Initial SOC: $SOC_{ini} = 0.452$

TABLE 2. Ramp rate model parameters used in simulation.

DESCRIPTION	SYMBOL	VALUE	
Active power (up and down) ramp rate limit in the POI, p.u./s.	RR_{max} and RR_{min}	50 kW/min (*)	0.000757 pu/s
		100 kW/min (*)	0.001515 pu/s
		150 kW/min (**)	0.00227 pu/s
Maximum SOC, p.u.	SOC_{max}	0.9	
Minimum SOC, p.u.	SOC_{min}	0.2	
BESS rated charging/ discharging time (s)	T	1496.2	
BESS lag time constant (s)	T_{p_K}	0.02	
Freeze lag time constant (s)	T_p	0.0001	
Ramp rate controller lag time constant (s)	T_{lag}	0.02	
Ramp Rate controller proportional gain, p.u.	$K_{p_{RR}}$	0.12002	
Ramp Rate controller integral gain, p.u.	$K_{i_{RR}}$	0.73842	
PV active power base (MW)	P_{PV}^{base}	1.1	
BESS active power base (MW)	P_{Bess}^{base}	0.95	
Best Variable Gain Parameters	$[P_1, P_2, P_3, P_4]$	[0.0011, 0.7158, 0.9520, 0.9325]	

* 50 kW/min → 0.05 MW/min → ((0.05/1.1)/60) = 0.000757 pu/s
* 100 kW/min → 0.10 MW/min → ((0.1/1.1)/60) = 0.001515 pu/s
*** 150 kW/min → 0.15 MW/min → ((0.15/1.1)/60) = 0.002273 pu/s.

TABLE 3. WECC model flag parameters used in simulation.

DESCRIPTION	NAME	VALUE
Constant Q (=0) or local power factor (=1) control	$PF\ Flag$	0
Local Q (=0) or voltage control (=1)	$V\ flag$	1
Bypass (=0) or engage (=1) inner voltage regulator loop	$Q\ flag$	0
Power reference flag for solar PV plant	$P\ flag$	1
Priority to reactive current (=0) or active current (=1)	$PQ\ flag$	0
Plant-level reactive power (=0) or voltage control (=1)	$Ref\ flag$	0
Ramp Rate Control enable (=0), or Governor response enable (=1)	$FreqFlag$	0

- SOC bounds: $SOC_{max} = 0.9$, $SOC_{min} = 0.2$
- SCADA data: 1-second intervals
- Anatem integration step: 50 ms
- Simulation duration: approximately 30,000 - 38,200 seconds

III. RESULTS AND DISCUSSION

This section presents and discusses the results of optimizing SOC models using real data from a hybrid PV-BESS plant.

A. INPUT CURVE ANALYSIS

The input curves (Figs. 7 and 8) provide a detailed view of the ramp rate control dynamics of the system at POI. Fig. 7 illustrates the measured and calculated active power at both the POI and the PV system on the base day, with the ramp rate set at 100 kW/min. This visualization illustrates how the BESS actively compensates for the PV output fluctuations, ensuring that the total power delivered at the POI adheres to the ramp rate constraint.

Fig. 8 further demonstrates the measured and calculated active power from the BESS itself, reinforcing the system's ability to smooth out PV variability and maintain ramp-rate compliance. Together, these figures confirm the effectiveness of the control strategy and importance of precise signal selection for robust ramp rate management in hybrid PV-BESS plants.

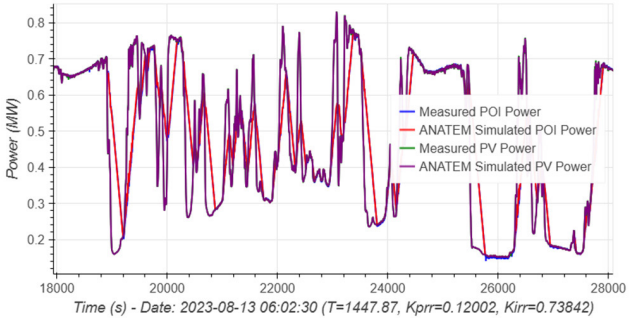

FIGURE 7. Active power measured and calculated at the POI and PV (Base Day, 100 kW/min).

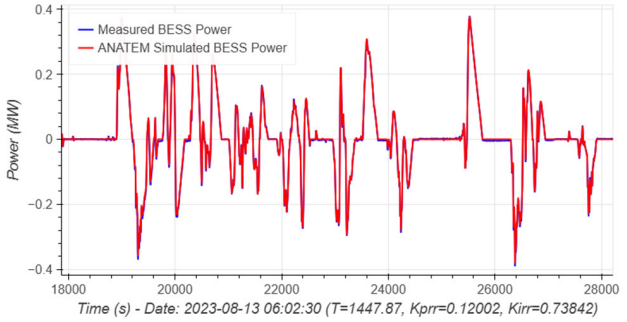

FIGURE 8. Active power measured and calculated from the BESS (Base Day, 100 kW/min).

B. GENERIC MODEL OPTIMIZATION

Optimization of the generic SOC model via DE yielded a consistent time constant of T = 1447.84, with minimal variation across 20 independent runs (≈0.015%), indicating strong convergence. This process is illustrated in Fig. 9, where the interquartile range is very narrow and the best-performing run (round 8) lies nearly on top of the median, demonstrating the robustness of the optimization.

Fig. 10 shows the RMSE values for the same 20 runs. The similarly narrow dispersion and alignment between the median and the best round confirm the statistical stability and consistent convergence of the DE algorithm.

Fig. 11 compares the measured SOC with the SOC simulated using the generic model on the base day. Noticeable deviations occur during fast charge–discharge transitions,

FIGURE 9. Distribution of optimal T parameter across rounds (Generic model).

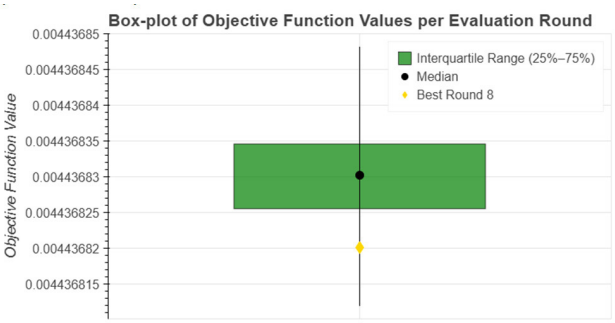

FIGURE 10. RMSE results for 20 optimization rounds (Generic model).

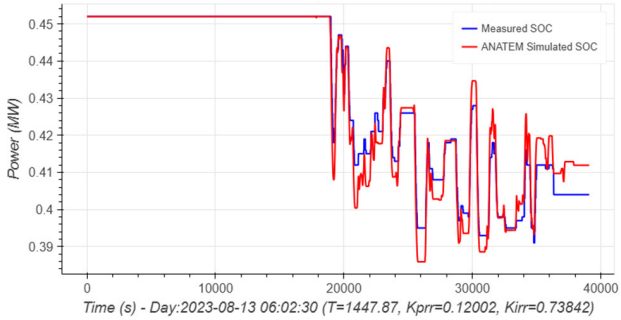

FIGURE 11. Comparison of measured and simulated SOC (Generic model, Base Day).

showing that the fixed-gain integrator cannot adequately follow rapid SOC dynamics. These discrepancies become more pronounced under high ramp-rate conditions, indicating limited adaptability of the generic model in nonlinear operating regimes.

Table 4 complements this analysis by summarizing the statistical metrics for both the optimized time constant (T) and the corresponding RMSE values.

RMSE represents the average error between measured and simulated SOC profiles for the best solution in each optimization round, expressed in per unit (pu). The standard deviation was calculated over the RMSE values obtained from all 20 rounds, quantifying the dispersion of RMSE across independent runs. The coefficient of variation (CV) was computed as (standard deviation/mean RMSE) × 100%, providing a normalized measure of variability. The small

TABLE 4. Statistical summary of optimized time constant (T) and RMSE across 20 DE rounds.

Parameter	Best	Mean	Standard Deviation	Coefficient of Variation (%)
RMSE (pu)	*0.00399*	*0.00444*	*6.00E-09*	*0.00014*
T (s)	*1447.87*	*1448.01*	*0.21610*	*0.01492*

standard deviation and CV reflect the high consistency and stability of the optimization process, as the DE algorithm converged to similar solutions in each round. The accuracy of the RMSE value is further confirmed by the narrow spread shown in Fig. 9.

All results in Table 4 were obtained using a fixed random seed to ensure reproducibility.

C. VARIABLE GAIN MODEL OPTIMIZATION

The variable gain SOC model was optimized using DE, yielding the parameter set $P_1 = 0.0011$, $P_2 = 0.7158$, $P_3 = 0.9520$, and $P_4 = 0.9325$, which correspond to the lowest RMSE among the 20 independent optimization rounds. These values remained consistent across runs and produced a substantially lower RMSE than the generic model. The integration time constant was fixed at T = 1496.2, as determined from (3), reflecting the physical characteristics of the equivalent BESS system.

Fig. 12 shows the piecewise-linear gain function k_p^{var} as a function of P_{Bess} (pu). The function is continuous at the breakpoints and transitions smoothly between constant-gain regions and a linear mid-range. This dynamic adjustment enhances SOC tracking accuracy under varying charge-discharge conditions.

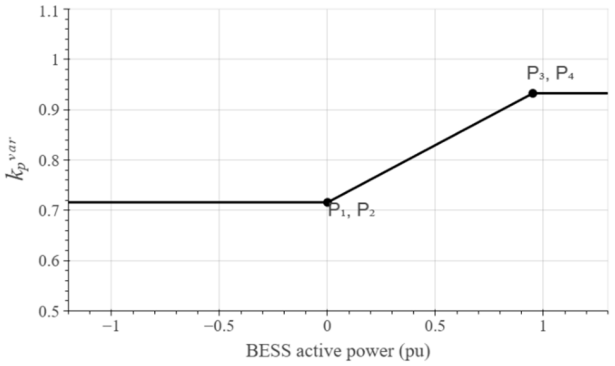

FIGURE 12. Piecewise-linear gain function k_p^{var} versus P_{BESS} (pu) for the optimized parameters.

Fig. 13 depicts the variability of the four ramp-function parameters across the 20 runs. Parameters P_2 and P_4 exhibit very low dispersion, indicating stable identification of the low- and high-power gain plateaus. Parameter P_1 also exhibits low absolute variability, remaining confined to a narrow range close to zero; the higher CV% results only from its small magnitude and does not reflect instability. In contrast, P_3 presents wider dispersion, although its effect on SOC

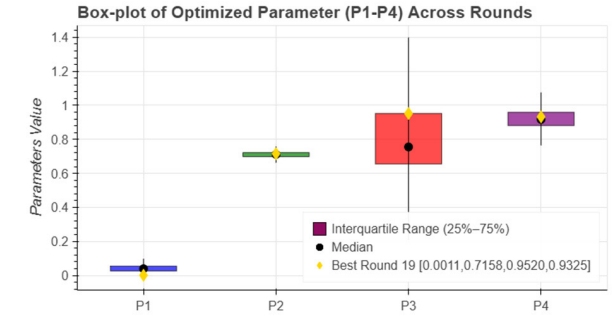

FIGURE 13. Distribution of optimal parameters P1–P4 across rounds(Variable gain model).

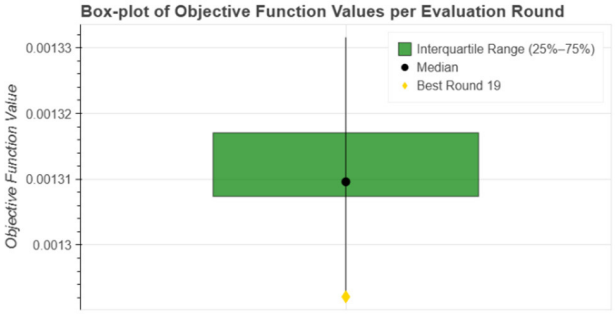

FIGURE 14. RMSE results for 20 Optimization Rounds (Variable gain).

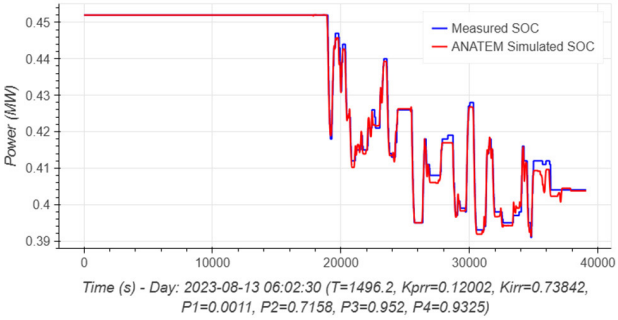

FIGURE 15. Comparison of measured and simulated SOC (Variable gain model, Base Day).

accuracy is mitigated by the nearly constant gain imposed by P4 in the upper power region. Overall, the piecewise-linear structure remains robust under varying operating conditions, with P_1, P_2, and P_4 showing strong parameter stability.

Fig. 14 shows the RMSE values across the optimization rounds. The narrow interquartile range and the close alignment between the median and the best-performing run confirm the stability and improved accuracy of the variable-gain formulation.

Fig. 15 compares the measured SOC with the SOC simulated using the optimized variable-gain model. The simulated profile closely follows the measured SOC, including during deep charge and discharge events, demonstrating the model's ability to adapt its integration gain and accurately track rapid SOC dynamics.

TABLE 5. Comparative evaluation of SOC tracking accuracy using RMSE across ramp-rate scenarios (Variable gain model).

Parameter	Best	Mean	Standard Deviation	Coefficient of Variation (%)
RMSE	*0.00142*	*0.00131*	*1.11E-05*	*0.84825*
P1	*0.0011*	*0.04117*	*0.02660*	*64.5960*
P2	*0.7158*	*0.70976*	*0.01257*	*1.77153*
P3	*0.9520*	*0.78365*	*0.15868*	*20.2488*
P4	*0.9325*	*0.92028*	*0.05375*	*5.84064*

TABLE 6. Comparative evaluation of SOC tracking accuracy using RMSE across ramp-rate scenarios using the best parameters.

Day	Ramp Rate (kW/min)	RMSE Generic Model	RMSE Variable Gain	Δ_{RMSE} (%)
Base Day	*100*	0.00399	0.00142	64.4%
Test Day1	*100*	0.02328	0.00696	70.1%
Test Day2	*100*	0.00582	0.00194	66.7%
Test Day3	*100*	0.01686	0.00325	80.7%
Test Day4	*110*	0.03399	0.00533	84.3%
Test Day5	*110*	0.00848	0.00284	66.5%
Test Day6	*110*	0.00342	0.00126	63.1%
Test Day7	*110*	0.00433	0.001517	65.0%
Test Day8	*110*	0.02382	0.002068	91.3%
Test Day9	*50*	0.01775	0.003854	78.3%
Test Day10	*50*	0.01392	0.005923	57.4%
Test Day11	*50*	0.01068	0.001670	84.4%

Notes:
1. Positive Δ_{RMSE}% indicates improved SOC-tracking accuracy with the variable-gain model relative to the generic model.
2. A higher positive Δ_{RMSE}% reflects greater improvement.

Table 5 summarizes the statistical metrics for the best value, mean, standard deviation and coefficient of variation for the RMSE and the four calibrated parameters. These results confirm the effectiveness of the variable-gain model in representing nonlinear SOC behavior. Overall, the adaptive gain mechanism reduces the SOC-tracking RMSE by up to 64% compared with the generic model on the base day.

D. RMSE SUMMARY AND TABLE EVALUATION

Table 6 reports the SOC-tracking RMSE for the generic and variable gain models across the 11 validation days and the three ramp-rate configurations. For methodological consistency, each model uses its best-performing parameter set obtained on the base day, and these parameters are kept fixed for all subsequent validation days.

Across the 11 validation days, the percentage improvement (Δ_{RMSE}) ranges from 57.4% to 91.3%, with a mean of 71.5% and a standard deviation of 10.5%, as defined by (9). These results indicate that the proposed formulation reduces the average SOC-tracking error under normal operating conditions, regardless of the daily PV profile or the ramp-rate limit. Representative SOC-tracking curves, including the highest-

TABLE 7. Comparison of SOC tracking accuracy using best parameters for generic and variable gain models.

Day	Measured and Simulated Active Power from BESS	Generic Model – Measured and Simulated SOC	Variable Gain Model – Measured and Simulated SOC
Test Day 3 *100 kW/min* Δ_{RMSE} =80.7%	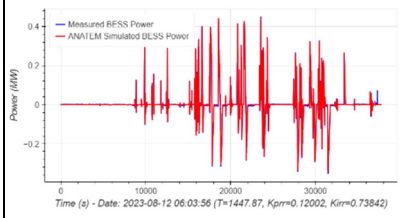	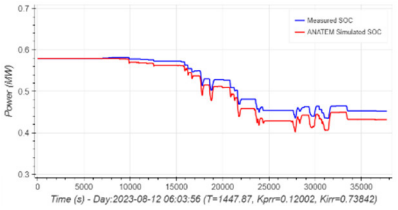	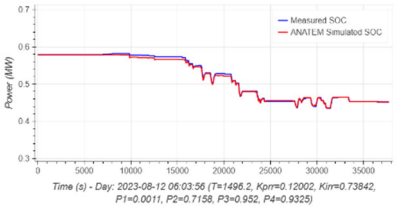
Test Day 4 *110 kW/min* Δ_{RMSE} =84.3%	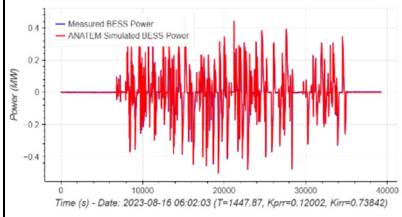	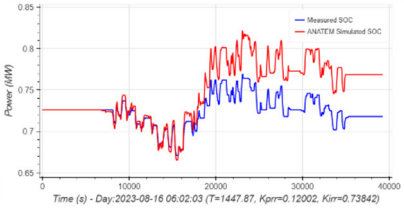	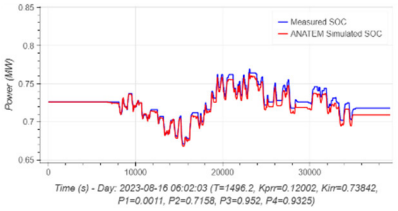
Test Day 8 *110 kW/min* Highest Δ_{RMSE} =91.3%	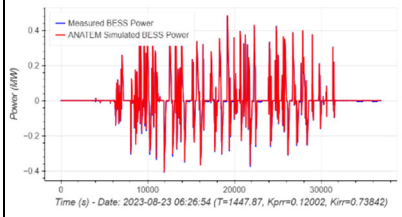	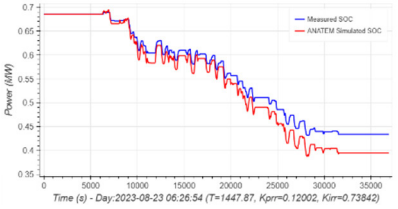	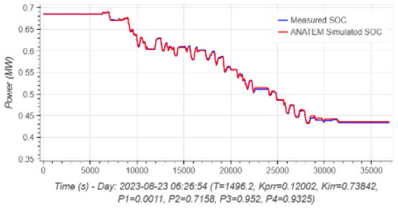
Test Day 10 *50 kW/min* Lowest Δ_{RMSE} =57.4%	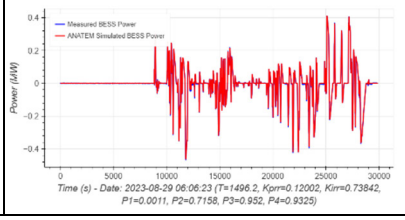	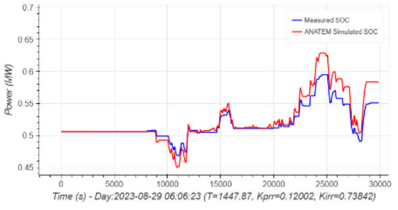	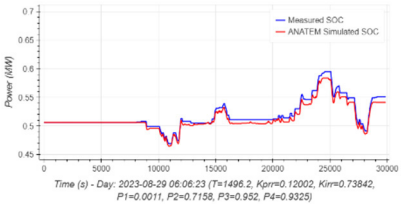

and lowest-improvement cases, are shown in Table 7 (see Appendix B).

$$\Delta_{RMSE} = \left(\frac{RMSE_{generic\ model} - RMSE_{variable\ gain}}{RMSE_{generic\ model}} \right) \times 100\% \tag{9}$$

Although RMSE concisely measures average accuracy, it does not capture timing misalignment, transient deviations, or systematic bias. Therefore, Table 8 extends the assessment with complementary dynamic indicators: mean error (ME), SOC timing lag, and peak SOC error during fast transitions.

E. RESIDUAL AND DYNAMIC VALIDATION BEYOND RMSE

A residual-based dynamic validation was performed to complement the RMSE-based analysis. The evaluation includes the SOC residual time series (measured minus simulated SOC), residual histograms, and three metrics:

- Mean Error (ME) to detect bias,
- Timing Lag, from maximum cross-correlation to assess temporal alignment, and
- Peak SOC Error during fast SOC transitions (95th-percentile threshold).

TABLE 8. Dynamic SOC-tracking metrics for generic and variable-gain models.

Day	Ramp Rate kW/min	Generic Model SOC ME (pu)	Generic Model SOC Lag (s)	Generic Model SOC Peak (pu)	Variable Gain SOC ME (pu)	Variable Gain SOC Lag (s)	Variable Gain SOC Peak (pu)
Base Day	*100*	0.00002	15	0.0129	0.00043	9	0.0084
Test Day1	*100*	-0.01592	0	0.0481	0.00461	0	0.0171
Test Day2	*100*	-0.00306	7	0.0152	0.00118	6	0.0069
Test Day3	*100*	0.01386	0	0.0354	0.00169	0	0.0095
Test Day4	*110*	-0.02506	14	0.0585	0.00405	14	0.0126
Test Day5	*110*	-0.00228	15	0.0242	0.00180	10	0.0100
Test Day6	*110*	-0.00001	12	0.0131	-0.00043	12	0.0065
Test Day7	*110*	0.00254	0	0.0197	0.00106	0	0.0069
Test Day8	*110*	0.01895	0	0.0447	-0.00073	0	0.0066
Test Day9	*50*	-0.00654	18	0.0298	0.00120	13	0.0115
Test Day10	*50*	-0.00627	4	0.0364	0.00455	9	0.0154
Test Day11	*50*	0.00918	0	0.0199	0.00118	0	0.0074

Notes:
1. SOC ME: mean SOC residual (measured − simulated).
2. SOC Lag: timing offset obtained from the maximum cross-correlation between measured and simulated SOC (positive = simulation lag).
3. SOC Peak Error: maximum absolute SOC residual during fast SOC transitions (95th-percentile threshold).

Across all validation days, residuals are centered near zero with limited dispersion, indicating the absence of drift. Table 8 summarizes these metrics for both models. The variable-gain formulation consistently yields lower peak SOC errors, typically 40% to 70% below those of the generic model, and exhibits reduced or comparable timing lag, frequently below 10 s, whereas the generic model reaches up to 18 s. Both models show negligible bias, with ME values close to zero. Overall, the variable-gain model not only reduces the average deviation reported in Table 6 but also improves dynamic fidelity by maintaining tighter tracking during rapid transitions and better temporal synchronization with measurements.

Although both models performed well under normal operating conditions, extreme cases such as deep cycling near SOC limits or highly abrupt power swings could not be fully assessed because the available dataset was collected during a plant revamp period with additional supervisory interventions. Future work will include targeted experiments and expanded datasets to evaluate robustness under high-stress conditions and across different battery chemistries.

IV. CONCLUSION

This study proposed and validated a methodology for tuning SOC models in hybrid PV–BESS systems using real operational data and Differential Evolution optimization. The generic SOC model, which is based on a fixed integration time constant, showed limited accuracy under dynamic operating conditions. In contrast, the proposed variable gain model introduced a dynamic adjustment mechanism that significantly enhanced the SOC tracking performance, particularly during periods of rapid power fluctuation.

The simulation results demonstrated the robustness of the variable gain model across different ramp-rate configurations and operational days. Across all validation scenarios, the variable gain formulation reduced SOC-tracking RMSE by 57.4% to 91.3%, while also decreasing timing lag and reducing peak SOC deviations during fast transients. Key findings include:

- consistently lower RMSE relative to the fixed-gain model.
- the importance of dynamic gain adaptation for accurate SOC modeling under variable conditions.
- the efficiency and scalability of the vectorized DE-based optimization framework.

The proposed methodology is not restricted to PV–BESS applications. It can be extended to other hybrid systems and to the calibration of control functions that require tuning using real operational data. This is particularly relevant in Brazil, where recent events have emphasized the importance of accurate dynamic models to ensure grid stability. Applying this approach to larger-scale BESS installations and different hybrid configurations may further validate its robustness and practical value.

It should be noted that the equivalent model adopted in this study jointly represents the AC/DC converter and the battery, which prevents the separation of nonlinear effects such as temperature dependence, voltage-dependent capacity, and state-of-health evolution. The identification and modeling of these phenomena represent natural directions for future developments as more detailed subsystem measurements become available.

Additionally, extreme operating conditions, such as deep cycling near SOC limits or abrupt power ramps, could not be fully assessed due to the lack of clean and reproducible data during the plant revamp period. Future work will incorporate controlled experiments to evaluate model behavior under high-stress conditions and for different battery chemistries.

The next phase of this research will focus on applying the proposed SOC-modeling and tuning methodology to industrial-scale BESS deployments, including behind-the-meter applications in refinery environments. This will enable detailed analysis of battery cycling and SOH evolution under real operating conditions and support both operational reliability and the provision of ancillary services. The methodology will also be explored in system operation and planning studies, including optimal battery sizing and integration strategies, with planned collaborations with system operators to validate the approach at larger scales and in diverse regulatory contexts.

APPENDIX A
RAMP RATE AND WECC MODEL PARAMETERS

See Tables 2 and 3.

APPENDIX B
SOC TRACKING RESULTS FOR SELECTED TEST DAYS

This appendix presents the selected results from the simulation campaign in Table 7, focusing on the SOC tracking performance of both generic and variable gain models. The input data corresponded to the measured active power injected or absorbed by the BESS on specific operational days. The table summarizes the comparison between the measured and simulated SOC responses using best parameters for each model, highlighting the accuracy improvements achieved by the proposed variable gain approach.

All residual analyses in Tables 9 and 10 refer exclusively to the SOC residual, defined as:

$$e(t) = SOC_{measured}(t) - SOC_{simulated}(t).$$

The histograms therefore represent the statistical distribution of the SOC tracking error.

TABLE 9. Summary of SOC residual histogram characteristics.

Day	Generic Model – Histogram of SOC Residuals	Variable Gain Model – Histogram of SOC Residuals
Base Day $\Delta_{RMSE} = 64.4\%$	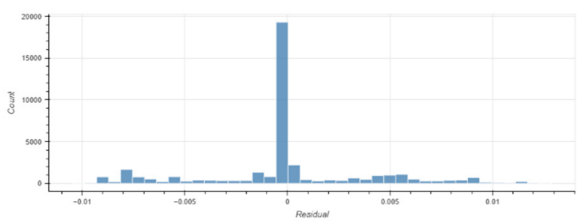	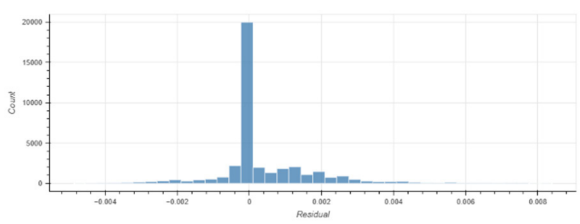
Test Day 8 $\Delta_{RMSE} = 91.3\%$	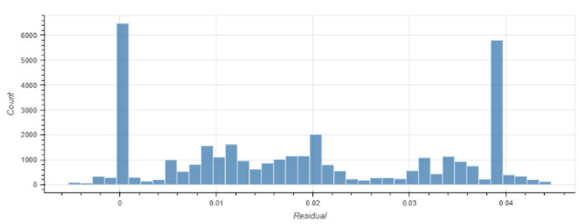	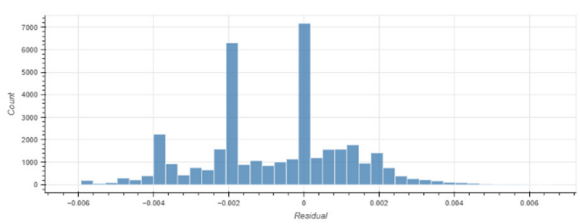
Test Day 10 $\Delta_{RMSE} = 57.4\%$	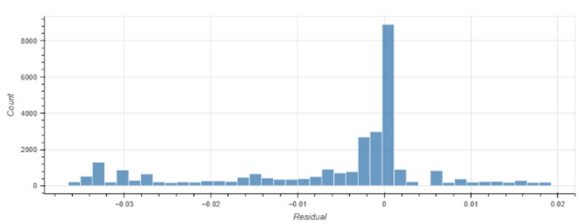	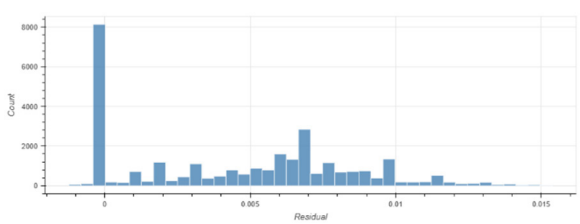

TABLE 10. Comparative SOC residual time-series summary.

Day	Generic Model – Temporal behavior of SOC residuals	Variable Gain Model – Temporal behavior of SOC residuals
Base Day $\Delta_{RMSE} = 64.4\%$	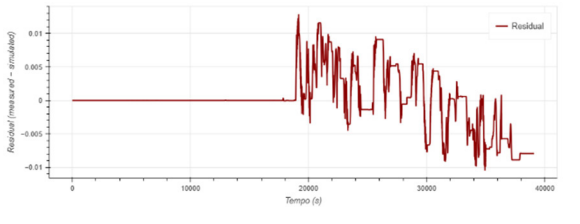	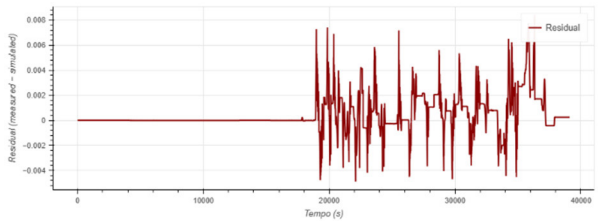
Test Day 8 $\Delta_{RMSE} = 91.3\%$	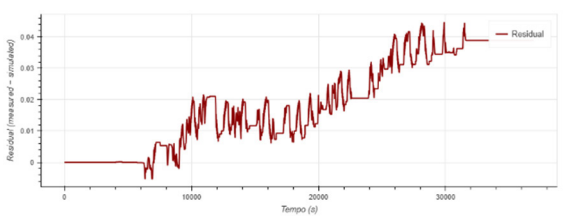	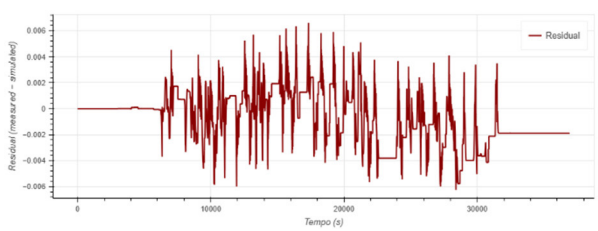
Test Day 10 $\Delta_{RMSE} = 57.4\%$	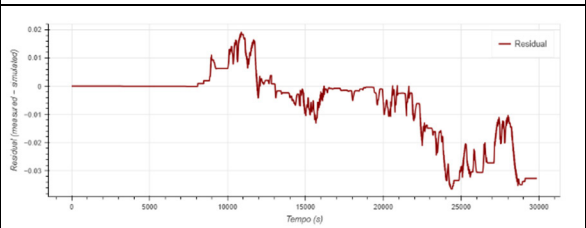	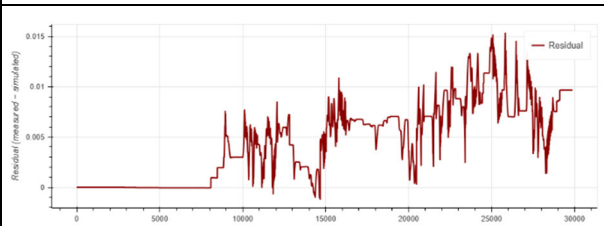

REFERENCES

[1] N. G. Chatzigeorgiou, S. Theocharides, G. Makrides, and G. E. Georghiou, "A review on battery energy storage systems: Applications, developments, and research trends of hybrid installations in the end-user sector," *J. Energy Storage*, vol. 86, May 2024, Art. no. 111192, doi: 10.1016/j.est.2024.111192.

[2] S. Chavhan, V. Mohale, and M. Kumbhar, "A review of recent advancements and challenges in battery energy storage system (BESS)," in *Proc. 1st Int. Conf. Innov. Sustain. Technol. Energy, Mechatronics, Smart Syst. (ISTEMS)*, Apr. 2024, pp. 1–6, doi: 10.1109/istems60181.2024.10560221.

[3] C. Zhao, P. B. Andersen, C. Træholt, and S. Hashemi, "Grid-connected battery energy storage system: A review on application and integration," *Renew. Sustain. Energy Rev.*, vol. 182, Aug. 2023, Art. no. 113400, doi: 10.1016/j.rser.2023.113400.

[4] *Executive Summary of the Medium-term Electrical Operation Plan of the SIN–PAR/PEL 2023–Cycle 2024-2028*, Nat. Electr. Syst. Operator (ONS), Rio de Janeiro, Brazil, 2023.
[5] H. Tahir, "Optimization of energy storage systems for integration of renewable energy sources—A bibliometric analysis," *J. Energy Storage*, vol. 94, Jul. 2024, Art. no. 112497, doi: 10.1016/j.est.2024.112497.
[6] P. Pourbeik, J. J. Sanchez-Gasca, J. Senthil, J. D. Weber, P. Zadkhast, Y. Kazachkov, S. Tacke, J. Wen, and A. Ellis, "Generic dynamic models for modeling wind power plants and other renewable technologies in large-scale power system studies," *IEEE Trans. Energy Convers.*, vol. 32, no. 3, pp. 1108–1116, Sep. 2017, doi: 10.1109/TEC.2016.2639050.
[7] G. Lammert, L. D. P. Ospina, P. Pourbeik, D. Fetzer, and M. Braun, "Implementation and validation of WECC generic photovoltaic system models in DIgSILENT PowerFactory," in *Proc. IEEE Power Energy Soc. Gen. Meeting (PESGM)*, Jul. 2016, pp. 1–5, doi: 10.1109/PESGM.2016.7741608.
[8] F. Fachini, L. Vanfretti, M. de Castro, T. Bogodorova, and G. Laere, "Modeling and validation of renewable energy sources in the OpenIPSL modelica library," in *Proc. 47th Annu. Conf. IEEE Ind. Electron. Soc.*, Oct. 2021, pp. 1–6, doi: 10.1109/IECON48115.2021.9589148.
[9] P. Pourbeik, J. J. Sanchez-Gasca, J. Senthil, J. Weber, P. Zadkhast, D. Ramasubramanian, S. D. Rao, J. Bloemink, R. Majumder, S. Zhu, D. Tucker, and S. Wang, "A generic model for inertia-based fast frequency response of wind turbines and other positive-sequence dynamic models for renewable energy systems," *IEEE Trans. Energy Convers.*, vol. 39, no. 1, pp. 425–434, Mar. 2024, doi: 10.1109/TEC.2023.3315058.
[10] P. F. Torres, G. Figueiredo, M. P. Almeida, A. R. A. Manito, J. C. S. Almeida Neto, M. A. R. Cassares, and R. Zilles, "Modelo dinâmico de sistemas de armazenamento de energia em baterias para provimento de Serviços ancilares," *Eletrônica de Potência*, vol. 28, no. 2, pp. 94–106, May 2023, doi: 10.18618/rep.2023.2.0036.
[11] P. Pourbeik et al., "Value and limitations of the positive sequence generic models of renewable energy systems," in *Proc. WECC Model. Valid. Work. Group*, Dec. 2015. Accessed: May 10, 2025. [Online]. Available: https://www.wecc.org/wecc-document/13511
[12] NERC Inverter-Based Resource Performance Working Group. (Jun. 2023). *Reliability Guideline: Performance, Modeling, and Simulations of BPS-Connected Battery Energy Storage Systems and Hybrid Power Plants*. Based Resource Performance Working Group. [Online]. Available: https://www.nerc.com/comm/RSTC_Reliability_Guidelines/Reliability_Guideline_BESS_Hybrid_Performance_Modeling_Studies.pdf
[13] WECC. (Nov. 2016). *WECC Battery Storage Dynamic Modeling Guideline*. Accessed: Oct. 27, 2024. [Online]. Available: https://www.wecc.org/sites/default/files/documents/meeting/2024/WECC%20Battery%20Storage%20Guideline%20updates%204-7-17%20.pdf
[14] Y. Shi, S. Cheng, C. Chen, Y. Luo, J. Zhao, and M. Ghiasi, "Modified biogeography optimization strategy for optimal sizing and performance of battery energy storage system in microgrid considering wind energy penetration," *Batteries*, vol. 9, no. 5, p. 254, Apr. 2023, doi: 10.3390/batteries9050254.
[15] S. M. Maroufi, S. Karrari, K. Rajashekaraiah, and G. De Carne, "Power management of hybrid flywheel-battery energy storage systems considering the state of charge and power ramp rate," *IEEE Trans. Power Electron.*, vol. 40, no. 7, pp. 9944–9956, Jul. 2025, doi: 10.1109/TPEL.2025.3546013.
[16] B. Li and M. Ghiasi, "A new strategy for economic virtual power plant utilization in electricity market considering energy storage effects and ancillary services," *J. Electr. Eng. Technol.*, vol. 16, no. 6, pp. 2863–2874, Nov. 2021, doi: 10.1007/s42835-021-00811-8.
[17] A. Safari and H. Rahbarimagham, "An improved control strategy for managing reactive power and reducing capacity of interlinking converters by participating of electric vehicles in hybrid AC/DC microgrids," *IEEE Access*, vol. 13, pp. 17878–17894, 2025, doi: 10.1109/ACCESS.2025.3533110.
[18] F. L. Lirio, N. A. R. L. Netto, and L. R. da Silva. (Nov. 2024). *Manual Do Usuário Do Programa Anatem*. Cepel–Centro de Pesquisas de Energia Elátrica. [Online]. Available: https://see.cepel.br/manual/anatem/index.html#
[19] *Minimum Technical Requirements for the Connection of Battery Energy Storage Systems [Requisitos Técnicos Mínimos Para a Conexão De Sistemas De Armazenamento De Energia via Baterias]*, National Electric System Operator (ONS), Rio de Janeiro, Brazil, 2025.
[20] Manitoba HVDC Research Centre. (2025). *PSCAD®—Power Systems Computer Aided Design*. [Online]. Available: https://www.pscad.com/
[21] *Differential_evolution–SciPy V1.16.2 Manual*. Accessed: Sep. 23, 2025. [Online]. Available: https://docs.scipy.org/doc/scipy/reference/generated/scipy.optimize.differential_evolution.html
[22] *Solar Photovoltaic Power Plant Modeling and Validation Guideline*, Western Electricity Coordinating Council (WECC), Dec. 2019. Accessed: Oct. 27, 2024. [Online]. Available: https://www.wecc.org/sites/default/files/documents/meeting/2024/Solar%20PV%20Plant%20Modeling%20and%20Validation%20Guidline.pdf
[23] A. F. Schiochet, P. R. D. Monteiro, T. T. Borges, J. A. P. Filho, and J. G. de Oliveira, "Photovoltaic power intermittency mitigating with battery storage using improved WEEC generic models," *Energies*, vol. 17, no. 20, p. 5166, Oct. 2024, doi: 10.3390/en17205166.
[24] M. Yazdanpour, P. Taheri, A. Mansouri, and B. Schweitzer, "A circuit-based approach for electro-thermal modeling of lithium-ion batteries," in *Proc. 32nd Thermal Meas., Model. Manage. Symp. (SEMI-THERM)*, Mar. 2016, pp. 113–127, doi: 10.1109/SEMI-THERM.2016.7458455.
[25] D. J. Noelle, M. Wang, A. V. Le, Y. Shi, and Y. Qiao, "Internal resistance and polarization dynamics of lithium-ion batteries upon internal shorting," *Appl. Energy*, vol. 212, pp. 796–808, Feb. 2018, doi: 10.1016/j.apenergy.2017.12.086.
[26] C. Qiu, G. He, W. Shi, M. Zou, and C. Liu, "The polarization characteristics of lithium-ion batteries under cyclic charge and discharge," *J. Solid State Electrochemistry*, vol. 23, no. 6, pp. 1887–1902, Jun. 2019, doi: 10.1007/s10008-019-04282-w.

ANDRÉ FERNANDO SCHIOCHET was born in Brazil, in 1979. He received the B.Sc. degree in electrical engineering and the M.Sc. degree from the Federal University of Santa Catarina (UFSC), Santa Catarina, Brazil, in 2003 and 2006, respectively, and the master's degree in electrical equipment engineering applied to the oil and natural gas industry from Petrobras University, in 2009. He is currently pursuing the Ph.D. degree in electrical engineering with the Federal University of Juiz de Fora (UFJF), Minas Gerais, Brazil.

Since 2008, he has been with Petróleo Brasileiro S.A.—PETROBRAS, working as an Equipment Engineer with the Refining, Gas and Energy Project Engineering Division. His professional experience includes electrical studies, reliability analysis, and the integration of battery energy storage systems (BESS) in industrial environments. His current research interests include the deployment of BESS in refinery operations, optimal battery sizing, and the use of advanced control models to enhance system reliability and flexibility. His research interests include model development, control strategies for power systems, and the application of optimization methods in operational planning and ancillary services.

GUSTAVO JACQUES FRIEDRICH received the bachelor's degree in electrical engineering from the Federal University of Rio Grande do Sul (UFRGS), Brazil, in 2019. He is currently pursuing the master's degree in electrical engineering with Fluminense Federal University (UFF), Brazil. Since 2022, he has been with PETROBRAS as an Equipment Engineer. His research interests include renewable energy, power system dynamics, and optimization of electrical systems.

JOÃO ALBERTO PASSOS FILHO received the B.Sc. degree in electrical engineering and the M.Sc. degree from the Federal University of Juiz de Fora (UFJF), Brazil, in 1995 and 2000, respectively, and the D.Sc. degree in electrical engineering from COPPE, Federal University of Rio de Janeiro (UFRJ), Brazil, in 2005.

From 1997 to 2009, he was a Researcher with the Electric Energy Research Center (CEPEL), where he contributed to the development of software tools for power system analysis. Since 2009, he has been with the Department of Electrical Energy, UFJF, where he is involved in teaching and research activities. His primary research interests include power system security assessment, the integration of distributed energy resources, and the planning and control of electrical systems.

JANAíNA GONÇALVES DE OLIVEIRA received the B.Sc. degree in electrical engineering from the Federal University of Juiz de Fora (UFJF), Brazil, in 2007, and the Ph.D. degree in technology from Uppsala University, Sweden, in 2011.

She has experience in system control and the application of power electronics to renewable energy, energy storage, and real-time simulation. From 2012 to 2013, she was a Researcher in power systems and control with the GE Global Research Center, Rio de Janeiro. Since 2014, she has been an Adjunct Professor with the Faculty of Electrical Engineering, UFJF. Since 2022, she has also been an Associate Professor with Uppsala University, Sweden. Her research interests include control systems, power electronics applications, energy storage integration, and real-time simulation for renewable energy systems.

Coordenação de Aperfeiçoamento de Pessoal de Nível Superior (CAPES) - ROR identifier: 00x0ma614